A Connectome-wide Functional Signature for Trait Anger

M. Justin Kim[1,2], Maxwell L. Elliott[3], Annchen R. Knodt[3], & Ahmad R. Hariri[3]

[1]Department of Psychology, Sungkyunkwan University, Seoul, South Korea, [2]Center for Neuroscience Imaging Research, Institute for Basic Science, Suwon, South Korea, [3]Laboratory of NeuroGenetics, Department of Psychology and Neuroscience, Duke University, Durham, USA

Supplemental Methods

Image Acquisition

Each participant was scanned using one of the two identical research-dedicated GE MR750 3T scanner equipped with high-power high-duty-cycle 50-mT/m gradients at 200 T/m/s slew rate, and an eight-channel head coil for parallel imaging at high bandwidth up to 1MHz at the Duke-UNC Brain Imaging and Analysis Center. A semi-automated high-order shimming program was used to ensure global field homogeneity. A series of 34 interleaved axial functional slices aligned with the anterior commissure-posterior commissure plane were acquired for full-brain coverage using an inverse-spiral pulse sequence to reduce susceptibility artifacts (TR/TE/flip angle = 2000 ms/ 30 ms/ 60; FOV = 240 mm; 3.75 × 3.75 × 4 mm voxels; interslice skip=0). Four initial radiofrequency excitations were performed (and discarded) to achieve steady-state equilibrium. To allow for spatial registration of each participant's data to a standard coordinate system, high-resolution three-dimensional T1-weighted structural images were obtained in 162 axial slices using a 3D Ax FSPGR BRAVO sequence (TR/TE/flip angle = 8.148 ms / 3.22 ms / 12°; voxel size = 0.9375 × 0.9375 × 1 mm; FOV = 240 mm; interslice skip=0; total scan time = 4 min and 13 s). For each participant, two back-to-back 4-minute 16-second (256 time points) rsfMRI scans were acquired. Participants were instructed to remain awake, with their eyes open during each resting-state scan. Participants also completed an emotional

face-matching task (6:30 min, 195 time points), a card-guessing task (5:42 min, 171 time points), a working memory task (11:48 min, 354 time points), and a face-naming task (5:24 min, 162 time points). Summarized below are descriptions of the four experimental paradigms used for the task fMRI scans. We note that these descriptions are also available in our previous published work (Farber et al., 2019; Forbes et al., 2009; Kim et al., 2018).

Emotional Face-matching Task

The experimental fMRI paradigm consists of four blocks of a perceptual face-matching task interleaved with five blocks of a sensorimotor control task. The DNS version of this paradigm consists of one block each of fearful, angry, surprised, and neutral facial expressions presented in a pseudorandom order across participants. During face-matching blocks, participants view a trio of faces and select one of two faces (on the bottom) identical to a target face (on the top). Each face processing block consists of six images, balanced for gender, all of which were derived from a standard set of pictures of facial affect (Ekman & Friesen, 1976). During the sensorimotor control blocks, participants view a trio of simple geometric shapes (circles and vertical and horizontal ellipses) and select one of two shapes (bottom) that are identical to a target shape (top). Each sensorimotor control block consists of six different shape trios. All blocks are preceded by a brief instruction ("Match Faces" or "Match Shapes") that lasts 2 s. In the task blocks, each of the six face trios is presented for 4 s with a variable interstimulus interval (ISI) of 2-6 s (mean = 4 s) for a total block length of 48 s. A variable ISI is used to minimize expectancy effects and resulting habituation, and maximize amygdala reactivity throughout the paradigm. In the control blocks, each of the six shape trios is presented for 4 s with a fixed ISI of 2 s for a total block length of 36 s. Total task time is 390 s.

Card-guessing Task

Our blocked-design number-guessing paradigm consists of a pseudorandom presentation of three blocks of predominantly positive feedback (80% correct guess), three blocks of predominantly negative feedback (20% correct guess) and three control blocks. There are five trials in 3 seconds to guess, via button press, whether the value of a visually presented card is lower or higher than 5 (index and middle finger, respectively). The numerical value of the card is then presented for 500 milliseconds and followed by appropriate feedback (green upward-facing arrow for positive feedback; red downward-facing arrow for negative feedback) for an additional 500 milliseconds. A crosshair is then presented for 3 seconds, for a total trial length of 7 seconds. Each block comprises five trails, with three blocks each of predominantly positive feedback (80% correct) and three of predominantly negative feedback (20% correct) interleaved with three control blocks. During control blocks, participants are instructed to simply make button presses during the presentation of an "x" (3 seconds), which is followed by an asterisk (500 milliseconds) and a yellow circle (500 milliseconds). Each block is preceded by an instruction of "Guess Number" (positive or negative feedback blocks) or "Press Button" (control blocks) for 2 seconds resulting in a total block length of 38 seconds and a total task length of 342 seconds. Participants were unaware of the fixed outcome probabilities associated with each block and were led to believe that their performance would determine a net monetary gain at the end of the scanning session. Instead, all participants received $10. We included one incongruent trial within each task block (e.g., one of five trials during positive feedback blocks was incorrect resulting in negative feedback) to prevent participants from anticipating the feedback for each trial and to maintain participants' engagement and motivation to perform well.

Working Memory Task

An event-related working memory paradigm adapted from Tan et al. (2007). The paradigm included 10 trials for each of 6 different conditions, including 3 control conditions, consisting only of a 3s response phase, and 3 working memory (WM) conditions, consisting of a 0.5s encoding phase followed by a 4s maintenance interval and a 3s response phase. Control and WM conditions were interleaved with jittered rest intervals lasting 4s to 8.5s for a total scan length of 11m 48s. Responses were recorded via an MR-compatible button box using the index (left button) and middle (right button) fingers of the dominant hand. During the control conditions, participants performed 1) a simple motor task (M) in which they pressed either the left or the right button according to a prompt, 2) a numerical size judgment task (J) in which they chose the number on the left or right based on an instruction to choose either the larger or the smaller number, and 3) a numerical computation and size judgment task (CJ) in which they performed a numerical subtraction of 2 or 3 from either the left or right number, and made a numerical size judgment as instructed. In the first WM condition, participants viewed 2 numbers during the brief encoding phase, then recalled the numbers and performed a numerical size judgment as instructed (E_RJ). In the second WM condition, the participants additionally performed subtraction of 2 or 3 from one of the remembered numbers as indicated before making the numerical size judgment during recall (E_RCJ). In the final WM condition, participants performed subtraction of 2 or 3 from one of the 2 numbers during the brief encoding phase, then recalled the resulting two numbers and performed a numerical size judgment as instructed during the response phase after the maintenance interval (EC_RJ). In each WM condition trial, all the numbers were single digits from 0 to 9; the two numbers on which the numerical size judgment

was ultimately performed (after numerical computation if applicable) were equally balanced across 0 to 9, and equally likely to differ by either 1 or 3 units. Numerical computation was equally likely on the left or right number, with correct responses equally balanced on the left or right, and equally likely to be the larger or smaller number for each WM trial type. The trials were performed in an order that was optimized using a sequencing program (Wager & Nichols, 2003).

Face-naming Task

Our fMRI paradigm consists of the encoding and subsequent recall of novel face-name pairs (Zeineh et al., 2003). A distractor task (odd/even number identification) is interleaved between encoding and recall blocks to prevent maintenance of information in working memory. During each of four encoding blocks, subjects view six novel face-name pairs for 3.5 seconds each. During each of four recall blocks, subjects view six faces each presented for 2 seconds and immediately followed by an incomplete name fragment for 1 second during which they are required by forced-choice to determine if the fragment is correct or incorrect. A 1 second inter-trial interval is used during recall blocks. During each of four distractor blocks, subjects view six different numbers for 3.5 seconds each and are required to determine if the numbers are odd or even. Total task length is 324 seconds.

Image Processing

Anatomical images for each subject were skull stripped, intensity normalized, and nonlinearly warped to a study-specific average template in the standard stereotactic space of the Montreal Neurological Institute template using the advanced normalization tools (ANTs) SyN

registration algorithm (Klein et al., 2009). Time-series images for each subject were despiked, slice time corrected, realigned to the first volume in the time-series to correct for head motion using AFNI tools (Cox

registration (Greve & Fischl, 2009), spatially normalized into Montreal Neurological Institute space using the nonlinear ANTs SyN warp from the anatomical image, resampled to 2-mm isotropic voxels, and smoothed to minimize noise and residual difference in gyral anatomy with a Gaussian filter set at 6-mm full width at half maximum. All transformations were concatenated so that a single interpolation was performed.

Time-series images for each participant were further processed to limit the influence of motion and other artifacts. Voxelwise signal intensities were scaled to yield a time-series mean

orrection

parameters (3 rotation and 3 translation) and their first derivatives (Satterthwaite et al., 2013) yielding 12 motion regressors. White matter and cerebrospinal fluid nuisance regressors were created using CompCor (Behzadi, Restom, Liau, & Liu, 2007). Images were bandpass filtered to retain frequencies between 0.008 and 0.1 Hz, and volumes exceeding 0.25-mm framewise displacement or 1.55 standardized DVARS (Power, Mitra, Laumann, Snyder, Schlaggar, & Petersen, 2014) were censored. Nuisance regression, bandpass filtering, and censoring for each time- *3dTproject*.

Seed-based Analyses

MDMR identifies a set of ROIs with patterns of whole-brain connectivity associated with a variable of interest. However, the nature in which the connectivity of these MDMR-selected ROIs relates to said variable remains unclear. To address this, previous research using CWAS

(Elliott et al., 2018; Shehzad et al., 2014) has utilized traditional seed-based connectivity follow-up analyses to better understand the networks and brain regions that drive the associations discovered through MDMR. We followed the same procedure described in our previous work (Elliott et al., 2018). Namely, seed-based connectivity maps were created and correlation coefficients at each voxel were converted to *z* *r*-to-*z* transform. Then, correlations between these connectivity values and trait anger were calculated across the whole brain, with age and sex included as covariates. Importantly, these follow-up analyses do not represent independent statistical tests because they were performed *post hoc* to the family-wise error-controlled MDMR findings. Accordingly, these follow-up analyses were not thresholded to visualize all information that was relevant to the MDMR step. Finally, to characterize the overall MDMR seed-based functional connectivity patterns, functional connectivity estimates were summarized for each of seven previously identified canonical intrinsic networks (Yeo et al., 2011) to quantify the relative contributions of each network to the observed associations with trait anger.

Finally, seed-based analyses using *a priori* amygdala ROIs were performed, as the Power 264 atlas used in MDMR analyses does not cover the amygdala. Amygdala ROIs were defined using a high-resolution template generated from the 168 Human Connectome Project dataset (Tyszka & Pauli, 2016). For completeness, whole-brain functional connectivity analyses were performed separately for the basolateral (BL) and centromedial (CM) amygdala subregions in each hemisphere, yielding four amygdala ROIs. For this step, we followed the same procedures described above with the exception of implementing statistical thresholds, as these analyses do represent independent statistical tests from MDMR. Nonparametric permutation tests (n = 5,000) were performed on the data to determine significant voxels at $p < 0.05$ corrected for

multiple comparisons, using the *randomise* tool along with the threshold-free cluster enhancement method implemented in FSL (Smith and Nichols, 2009; Winkler et al., 2014).

References

Behzadi, Y., Restom, K., Liau, J., & Liu, T. T. (2007). A component based noise correction method (CompCor) for BOLD and perfusion based fMRI. *Neuroimage, 37,* 90-101. doi:10.1016/j.neuroimage.2007.04.042

Cox R. W. (1996). AFNI: software for analysis and visualization of functional magnetic resonance neuroimages. *Computational Biomedical Research, 29,* 162-173. doi:10.1006/cbmr.1996.0014

Ekman, P., & Friesen, W. (1976). *Pictures of Facial Affect*. Palo Alto, CA: Consulting Psychologists Press.

Elliott, M. L., Romer, A., Knodt, A. R., & Hariri, A. R. (2018). A connectome-wide functional signature of transdiagnostic risk for mental illness. *Biological Psychiatry, 84,* 452-459. doi:10.1016/j.biopsych.2018.03.012

Farber, M. J., Kim, M. J., Knodt, A. R., & Hariri, A. R. (2019). Maternal overprotection in childhood is associated with amygdala reactivity and structural connectivity in adulthood. *Developmental Cognitive Neuroscience, 40,* 100711.

Forbes, E. E., Brown, S. M., Kimak, M., Ferrell, R. E., Manuck, S. B., & Hariri, A. R. (2009). Genetic variation in components of dopamine neurotransmission impacts ventral striatal reactivity associated with impulsivity. *Molecular Psychiatry 14,* 60-70.

Greve, D. N., & Fischl, B. (2009). Accurate and robust brain image alighnment using boundary-based registration. *Neuroimage, 48,* 63-72. doi:10.1016/j.neuroimage.2009.06.060

V. (2009). Evaluation of 14 nonlinear deformation algorithms applied to human brain MRI registration. *Neuroimage, 46,* 786-802. doi:10.1016/j.neuroimage.2008.12.037

Kim, M. J., Scult, M. A., Knodt, A. R., Radtke, S. C., Brigidi, B. D., & Hariri, A. R. (2018). A link between childhood adversity and trait anger reflects relative activity of the amygdala and dorsolateral prefrontal cortex. *Biological Psychiatry: Cognitive Neuroscience and Neuroimaging, 3,* 644-649.

Power, J. D., Mitra, A., Laumann, T. O., Snyder, A. Z., Schlaggar, B. L., & Petersen, S. E. (2014). Methods to detect, characterize, and remove motion artifact in resting state fMRI. *Neuroimage, 84,* 320-341. doi:10.1016/j.neuroimage.2013.08.048

Wolf, D. H. (2013). An improved framework for confound regression and filtering for control of motion artifact in the preprocessing of resting-state functional connectivity data. *Neuroimage, 64,* 240-256. doi:10.1016/j.neuroimage.2012.08.052

Smith, S. M., & Nichols, T. E. (2009). Threshold-free cluster enhancement: addressing problems of smoothing, threshold dependence and localization in cluster inference. *Neuroimage, 44*, 83-98. http:/dx.doi.org/ 10.1016/j.neuroimage.2008.03.061

Tan, H.-Y., Chen, Q., Goldberg, T. E., Mattay, V. S., Meyer-Lindenberg, A., Weinberger, D. R., & Callicott, J. H. (2007). Catechol-O-methyltransferase Val158Met modulation of prefrontal-parietal-striatal brain systems during arithmetic and temporal transformations in working memory. *Journal of Neuroscience, 27*, 13393-401.

Tyszka, J. M., & Pauli, W. M. (2016). *In vivo* delineation of subdivisions of the human amygdaloid complex in a high-resolution group template. *Human Brain Mapping, 37*, 3979-3998. doi: 10.1002/hbm.23289

Wager, T. D., & Nichols, T. E. (2003). Optimization of experimental design in fMRI: A general framework using a genetic algorithm. *Neuroimage, 18*, 293-309.

Winkler, A. M., Ridgway, G. R., Webster, M. A., Smith, S. M., & Nichols, T. E. (2014). Permutation inference for the general linear model. *Neuroimage, 92*, 381 397. doi: 10.1016/j.neuroimage.2014.01.060

Zeineh, M. M., Engel, S. A., Thompson, P. M., & Bookheimer, S. Y. (2003). Dynamics of the hippocampus during encoding and retrieval of face-name pairs. *Science, 299*, 577-580.

Supplemental Tables

Table S1. Brain regions whose intrinsic functional connectivity with the left basolateral amygdala showed significant positive association with trait anger ($p < 0.05$, corrected for multiple comparisons across the whole brain).

Brain Region	Side	*Z*	*x*	*y*	*z*	# of voxels
Seed: Left Basolateral Amygdala						
Putamen	R	4.12	16	14	-2	10362
	L	4.01	16	12	-2	
Caudate	R	3.74	18	12	16	
	L	3.77	-18	8	16	
Nucleus Accumbens	R	3.11	6	12	-2	
	L	3.07	-6	12	-2	
Pallidum	R	3.83	18	-2	-6	
	L	3.55	18	0	-2	
Thalamus	R	3.53	20	-20	8	
Amygdala	R	3.01	24	0	-22	
Dorsomedial Prefrontal Cortex	R	4.69	6	58	34	6729
Dorsal Anterior Cingulate Cortex	R	3.22	6	30	18	
Inferior Frontal Gyrus	R	3.50	52	14	-2	236
Inferior Temporal Gyrus	L	4.47	-64	-18	-30	87
Middle Frontal Gyrus	L	3.29	-36	4	44	20
Temporal Pole	R	3.94	46	8	-44	15
Superior Frontal Gyrus	R	3.73	6	12	70	12
Orbitofrontal Gyrus	R	3.54	40	22	-18	11

Note: Coordinates are in Montreal Neurological Institute (MNI) space

Table S2. Brain regions whose intrinsic functional connectivity with the right basolateral amygdala showed significant positive association with trait anger ($p < 0.05$, corrected for multiple comparisons across the whole brain).

Brain Region	Side	*Z*	*x*	*y*	*z*	# of voxels
Seed: Right Basolateral Amygdala						
Inferior Frontal Gyrus	L	4.42	-38	16	20	13140
Dorsomedial Prefrontal Cortex	R	4.12	8	48	40	
Dorsal Anterior Cingulate Cortex	R	2.90	2	26	24	
Lateral Frontal Pole	R	3.60	46	56	6	
Medial Frontal Pole	R	3.68	8	64	-6	
Supplementary Motor Area	R	3.40	6	-12	72	
Lateral Occipital Cortex	R	3.81	46	-64	44	4036
	L	4.18	-38	-64	56	1335
	L	3.82	-62	-66	16	123
Inferior Temporal Gyrus	R	4.15	64	-18	-30	860
Middle Temporal Gyrus	R	3.39	68	-48	0	501
	L	3.94	-48	-6	-26	201
Brainstem	L	3.74	-10	-20	-22	443
	R	4.74	10	-20	-22	128
Cerebellum	R	4.02	2	-56	-46	425
Lateral Frontal Pole	L	3.45	-36	60	-4	346
	L	2.56	-46	46	6	22
Caudate	L	3.03	-18	14	14	266
	R	3.36	14	14	0	204
Superior Temporal Gyrus	L	3.67	-70	-34	4	215
Posterior Cingulate Cortex	R	3.84	10	-34	32	173

Thalamus	R	3.22	8	0	10	162
Supramarginal Gyrus	L	3.05	-68	-22	22	130
Hippocampus	R	3.48	20	-8	-26	40
Pallidum	L	2.94	-14	-8	-2	17
Thalamus	L	2.86	-10	0	-6	16
Amygdala	R	3.32	26	0	-22	11

Note: Coordinates are in Montreal Neurological Institute (MNI) space

Table S3. Brain regions whose intrinsic functional connectivity with the right centromedial amygdala showed significant positive association with trait anger ($p < 0.05$, corrected for multiple comparisons across the whole brain).

Brain Region	Side	*Z*	*x*	*y*	*z*	# of voxels
Seed: Right Centromedial Amygdala						
Inferior Frontal Gyrus	L	5.57	-36	16	20	22285
Dorsomedial Prefrontal Cortex	R	4.10	10	48	38	
Dorsal Anterior Cingulate Cortex	R	2.51	4	30	32	
Lateral Frontal Pole	R	3.36	50	56	4	
Medial Frontal Pole	R	3.56	8	66	-6	
Thalamus	R	3.76	12	-24	4	
Caudate	R	2.88	10	6	10	
	L	2.59	-16	8	16	
Amygdala	L	3.37	-20	-6	-12	
Nucleus Accumbens	R	2.96	12	16	-4	
Lateral Occipital Cortex	L	3.67	-38	-72	50	342
	L	3.44	-46	-62	28	158
	L	4.02	-62	-66	16	63
Orbitofrontal Cortex	L	3.37	-26	22	-26	277
Middle Temporal Gyrus	L	3.64	-50	-42	-2	263
	R	3.86	73	-29	1	146
	L	3.12	-58	-52	0	15
Temporal Pole	L	3.35	-58	10	0	144
Superior Temporal Gyrus	R	3.24	54	-8	-6	120
Supplementary Motor Area	R	3.53	14	-6	42	119
Inferior Temporal Gyrus	R	4.49	66	-18	-28	94

	R	3.50	60	-54	-20	14
Inferior Frontal Gyrus	R	3.33	60	18	-2	44
Precentral Gyrus	L	3.47	-54	0	20	37
Posterior Cingulate Cortex	R	3.35	10	-34	32	37
	L	2.84	-42	-24	2	25

Note: Coordinates are in Montreal Neurological Institute (MNI) space

Supplemental Figures

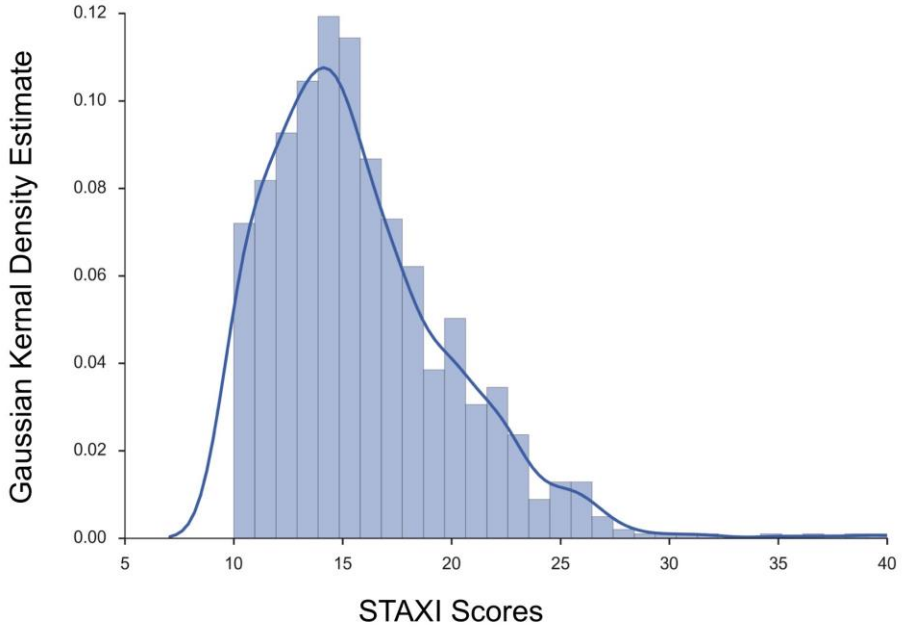

Figure S1. Histogram depicting the distribution of trait anger scores in the current study sample (*n* = 1,048).